Eur. Phys. J. A **31**, 373–381 (2007)
DOI 10.1140/epja/i2007-10003-9

THE EUROPEAN PHYSICAL JOURNAL A

Regular Article – Hadron Physics

Semi-Inclusive Deep Inelastic Scattering processes from small to large P_T

M. Anselmino[a], M. Boglione, A. Prokudin, and C. Türk

Dipartimento di Fisica Teorica, Università di Torino and INFN, Sezione di Torino, Via P. Giuria 1, I-10125 Torino, Italy

Received: 9 February 2007
Published online: 27 March 2007 –
Communicated by E. De Sanctis

Abstract. We consider the azimuthal and P_T-dependence of hadrons produced in unpolarized Semi-Inclusive Deep Inelastic Scattering (SIDIS) processes, within the factorized QCD parton model. It is shown that at small P_T values, $P_T \lesssim 1\,\mathrm{GeV}/c$, lowest-order contributions, coupled to unintegrated (transverse-momentum-dependent) quark distribution and fragmentation functions, describe all data. At larger P_T values, $P_T \gtrsim 1\,\mathrm{GeV}/c$, the usual pQCD higher-order collinear contributions dominate. Having explained the full P_T range of available data, we give new detailed predictions concerning the azimuthal and P_T-dependence of hadrons which could be measured in ongoing or planned experiments by HERMES, COMPASS and JLab Collaborations.

PACS. 13.88.+e Polarization in interactions and scattering – 13.60.-r Photon and charged-lepton interactions with hadrons – 13.85.Ni Inclusive production with identified hadrons

1 Introduction

In ref. [1] a comprehensive analysis of Semi-Inclusive Deep Inelastic Scattering (SIDIS) processes within a factorized QCD parton model at $\mathcal{O}(\alpha_s^0)$ was performed in a kinematical scheme in which the intrinsic tranverse momenta of the quarks inside the initial proton ($\boldsymbol{k}_\perp$) and of the final detected hadron with respect to the fragmenting quark ($\boldsymbol{p}_\perp$) were fully taken into account. The dependence of the unpolarized cross-section on the azimuthal angle ϕ_h between the leptonic and the hadron production plane (Cahn effect [2]) was compared to the available experimental data, and used to estimate the average values of $\langle k_\perp^2 \rangle$ and $\langle p_\perp^2 \rangle$. These values were adopted in modeling the intrinsic motion dependence of the quark distribution and fragmentation functions. This allowed a consistent description of the azimuthal dependence observed by HERMES and COMPASS Collaborations in SIDIS off transversely polarized protons [3,4], with the subsequent extraction [1,5] of the Sivers distribution function [6].

In ref. [1] the main emphasis, following the original idea of Cahn, was on the role of the parton intrinsic motion, with the use of unintegrated quark distribution and fragmentation functions. That applies to large-Q^2 processes, in a kinematical regime in which $P_T \simeq \Lambda_{\mathrm{QCD}} \simeq k_\perp$, where $P_T = |\boldsymbol{P}_T|$ is the magnitude of the final hadron transverse momentum. In this region QCD factorization with unintegrated distributions holds [7] and lowest-order QED elementary processes, $\ell\, q \to \ell\, q$, are dominating: the soft P_T of the detected hadron is mainly originating from quark intrinsic motion [8–10], rather than from higher-order pQCD interactions, which, instead, would dominantly produce large-P_T hadrons [11–14].

Indeed, a look at the results of ref. [1] (see, in particular, figs. 5 and 6) immediately shows that, while the inclusion of intrinsic $k_\perp$ and $p_\perp$ —coupled to lowest-order partonic interactions— leads to an excellent agreement with the data for small values of the transverse momentum P_T of the final hadron, it badly fails at higher P_T: the turning point is around $P_T \sim 1\,\mathrm{GeV}/c$. A similar conclusion was drawn in ref. [12]. The large-P_T region has been discussed at length in the literature and is related to contributions from higher-order QCD processes, like hard gluonic radiation and elementary scatterings initiated by gluons: these cannot be neglected when $P_T \gg \lambda_{\mathrm{QCD}}$ [11–14].

In this paper we start by showing that a complete agreement with data in the full range of P_T can be achieved; for $P_T \lesssim 1\,\mathrm{GeV}/c$ we follow the approach of ref. [1] —P_T originated by the intrinsic $k_\perp$ and $p_\perp$ with $\mathcal{O}(\alpha_s^0)$ partonic interaction— while in the range of $P_T \gtrsim 1\,\mathrm{GeV}/c$ we add the pQCD contributions —collinear partonic configurations with higher-order (up to $\mathcal{O}(\alpha_s^2)$) partonic interactions which generate the large P_T. We shall see that indeed most available data can be explained; the intrinsic $k_\perp$ contributions work well at small $P_T \lesssim 1\,\mathrm{GeV}/c$ and fail above that, while the higher-order

[a] e-mail: mauro.anselmino@to.infn.it

pQCD collinear contributions explain well the large $P_T \gtrsim 1\,\mathrm{GeV}/c$ data and fail, or are not even applicable, below that. The two contributions match in the overlapping region, $P_T \sim 1\,\mathrm{GeV}/c$, where it might be difficult to disentangle one from the other, as they describe the same physics. Infact parton intrinsic motions originate not only from confinement, but also from soft gluon emission, which, due to QCD helicity conservation, cannot be strictly collinear. Similar studies, concerning single transverse-spin asymmetries in Drell-Yan and SIDIS processes, with separate contributions —TMD quark distributions and higher-twist quark gluon correlations— in separate regions, have recently been published [15,16].

Having achieved such a complete understanding of the P_T-dependence of the SIDIS cross-sections we obtain a full confidence on the regions of applicability of the two approaches. We re-analyse the azimuthal dependence of the unpolarized cross-section —the Cahn effect, described in ref. [1]— which depends on quantities integrated over P_T. The actual data are dominated by the low-P_T contributions, and the results previously obtained remain valid; we obtain slightly different values of the parameters $\langle k_\perp^2 \rangle$ and $\langle p_\perp^2 \rangle$. We then consider running experiments (HERMES, COMPASS and experiments at JLab) and physical observables which are being or will soon be measured. They are mainly in the small-P_T regions and we give full sets of predictions for them.

The plan of the paper is the following: in sect. 2 we give a short overview of the kinematics and a collection of the basic formulae needed for the computation of the SIDIS cross-sections, both in the low-P_T approach of ref. [1] and in the pQCD large-P_T region; in sect. 3 we discuss and compare our results for $\mathrm{d}\sigma/\mathrm{d}P_T$, $\mathrm{d}\sigma/\mathrm{d}\phi_h$ and $\langle \cos\phi_h \rangle$ with the existing experimental data, over a very wide range of P_T values; in sect. 4 we give predictions for the forthcoming measurements of $\mathrm{d}\sigma/\mathrm{d}P_T$ and $\langle \cos\phi_h \rangle$ at HERMES, Compass and JLab. Some considerations on $\langle \cos 2\phi_h \rangle$ are made. Finally, in sect. 5 we draw our conclusions.

2 Kinematics and cross-sections

We consider SIDIS processes $\ell\, p \to \ell\, h\, X$ in the $\gamma^* p$ c.m. frame, as shown in fig. 1. The photon and the proton collide along the z-axis with momenta $\boldsymbol{q}$ and $\boldsymbol{P}$, respectively; the leptonic plane coincides with the x-z plane. We adopt the usual SIDIS variables (neglecting all masses):

$$s = (P+\ell)^2\,, \qquad (P+q)^2 = W^2 = \frac{1-x_{Bj}}{x_{Bj}}\,Q^2\,,$$
$$q^2 = -Q^2\,, \qquad x_{Bj} = \frac{Q^2}{2P\cdot q} = \frac{Q^2}{W^2+Q^2}\,,$$
$$y = \frac{P\cdot q}{P\cdot \ell} = \frac{Q^2}{x_{Bj}s}\,, \qquad z_h = \frac{P\cdot P_h}{P\cdot q}\,. \tag{1}$$

The SIDIS differential cross-section can schematically be written in terms of a perturbative expansion in orders of α_s as follows:

$$\mathrm{d}\sigma = \alpha_s^0\,\mathrm{d}\sigma_0 + \alpha_s^1\,\mathrm{d}\sigma_1 + \alpha_s^2\,\mathrm{d}\sigma_2 + \ldots\,, \tag{2}$$

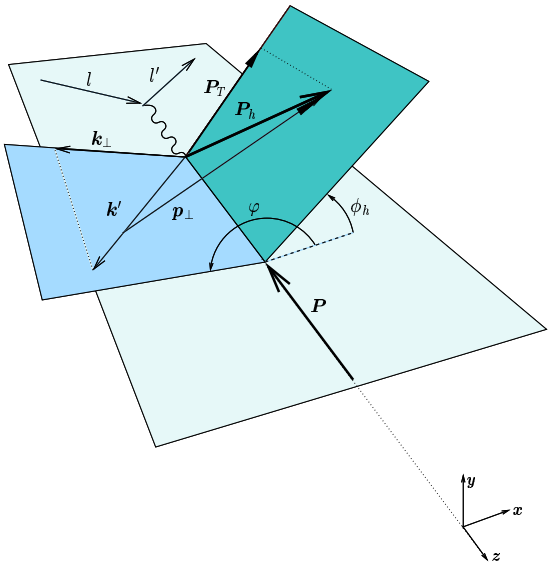

Fig. 1. Three-dimensional kinematics of the SIDIS process.

where $\mathrm{d}\sigma$ is a shorthand notation to indicate

$$\frac{\mathrm{d}^5\sigma^{\ell p\to \ell h X}}{\mathrm{d}x_{Bj}\,\mathrm{d}y\,\mathrm{d}z_h\,\mathrm{d}^2\boldsymbol{P}_T} = x_{Bj}s\,\frac{\mathrm{d}^5\sigma^{\ell p\to \ell h X}}{\mathrm{d}x_{Bj}\,\mathrm{d}Q^2\,\mathrm{d}z_h\,\mathrm{d}^2\boldsymbol{P}_T}\,. \tag{3}$$

The first term in this expansion is the lowest-order one; in the elementary interaction, $\ell\, q \to \ell\, q$, a virtual photon with four-momentum q strikes a quark which carries a transverse momentum $\boldsymbol{k}_\perp = k_\perp(\cos\varphi, \sin\varphi, 0)$ in addition to a fraction x of the light-cone proton momentum. The final detected hadron h originates from the fragmentation of the outgoing quark: $\boldsymbol{p}_\perp$ is the transverse momentum of h *with respect to the direction* of the fragmenting quark and z is the fraction of the light-cone quark momentum carried by the resulting hadron. Consequently, the detected hadron can have a transverse momentum $\boldsymbol{P}_T$ with a magnitude $P_T \simeq \langle k_\perp \rangle \simeq \langle p_\perp \rangle$. Indeed, this is the main source of hadrons with a small value of P_T [12,8–10].

Such a mechanism translates into a factorized [7] expression for the SIDIS cross-section, valid at all orders in $(k_\perp/Q)$:

$$\frac{\mathrm{d}^5\sigma_0^{\ell p\to \ell h X}}{\mathrm{d}x_{Bj}\,\mathrm{d}Q^2\,\mathrm{d}z_h\,\mathrm{d}^2\boldsymbol{P}_T} =$$
$$\sum_q \int \mathrm{d}^2\boldsymbol{k}_\perp\, f_q(x,\boldsymbol{k}_\perp)\,\frac{\mathrm{d}\hat\sigma^{\ell q\to \ell q}}{\mathrm{d}Q^2}\,J\,\frac{z}{z_h}\,D_q^h(z,\boldsymbol{p}_\perp) =$$
$$\sum_q e_q^2 \int \mathrm{d}^2\boldsymbol{k}_\perp\, f_q(x,\boldsymbol{k}_\perp)\,\frac{2\pi\alpha^2}{x_{Bj}^2 s^2}\,\frac{\hat s^2+\hat u^2}{Q^4}\,D_q^h(z,\boldsymbol{p}_\perp)$$
$$\times \frac{z}{z_h}\,\frac{x_{Bj}}{x}\left(1+\frac{x_{Bj}}{x}\,\frac{k_\perp^2}{Q^2}\right)^{-1}\,, \tag{4}$$

as explained in ref. [1], where the exact relationships between x, z, $\boldsymbol{p}_\perp$ and the observables x_{Bj}, z_h, $\boldsymbol{P}_T$ are given. Notice that at $\mathcal{O}(k_\perp/Q)$ one has $x_{Bj} = x$, $z_h = z$ and $\boldsymbol{P}_T = z\boldsymbol{k}_\perp + \boldsymbol{p}_\perp$. $f_q(x,\boldsymbol{k}_\perp)$ and $D_q^h(z,\boldsymbol{p}_\perp)$ are the parton density and the fragmentation function, respectively, for

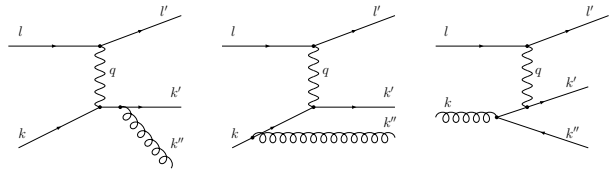

Fig. 2. Feynman diagrams corresponding to ℓq and ℓg elementary scattering at first order in α_s.

which we assume the usual x, $k_\perp$ or z, $p_\perp$ factorization, with a Gaussian $k_\perp$- and $p_\perp$-dependence:

$$f_q(x,\boldsymbol{k}_\perp) = f_q(x)\,\frac{1}{\pi\langle k_\perp^2\rangle}\,e^{-k_\perp^2/\langle k_\perp^2\rangle}\,,$$
$$D_q^h(z,\boldsymbol{p}_\perp) = D_q^h(z)\,\frac{1}{\pi\langle p_\perp^2\rangle}\,e^{-p_\perp^2/\langle p_\perp^2\rangle}\,, \qquad (5)$$

so that

$$\int \mathrm{d}^2\boldsymbol{k}_\perp\, f_q(x,\boldsymbol{k}_\perp) = f_q(x)\,,$$
$$\int \mathrm{d}^2\boldsymbol{p}_\perp\, D_q^h(z,\boldsymbol{p}_\perp) = D_q^h(z)\,. \qquad (6)$$

The integration over $\mathrm{d}^2\boldsymbol{k}_\perp$ in eq. (4) induces a dependence on $\cos\phi_h$ (at $\mathcal{O}(P_T/Q)$) and on $\cos 2\phi_h$ (at $\mathcal{O}(P_T/Q)^2$), where ϕ_h is the azimuthal angle of $\boldsymbol{P}_T$. The explicit expression, at $\mathcal{O}(P_T/Q)$, is given by:

$$\frac{\mathrm{d}^5\sigma^{\ell p\to\ell h X}}{\mathrm{d}x_{Bj}\,\mathrm{d}Q^2\,\mathrm{d}z_h\,\mathrm{d}^2\boldsymbol{P}_T} \simeq \sum_q \frac{2\pi\alpha^2 e_q^2}{Q^4}\,f_q(x_{Bj})\,D_q^h(z_h)$$
$$\times\left[1+(1-y)^2 - 4\,\frac{(2-y)\sqrt{1-y}\,\langle k_\perp^2\rangle\,z_h\,P_T}{\langle P_T^2\rangle\,Q}\,\cos\phi_h\right]$$
$$\times\,\frac{1}{\pi\langle P_T^2\rangle}\,e^{-P_T^2/\langle P_T^2\rangle}\,, \qquad (7)$$

where, $\langle P_T^2\rangle = \langle p_\perp^2\rangle + z^2\langle k_\perp^2\rangle$.

Let us now consider the contributions of order α_s, $\mathrm{d}\sigma_1$ in eq. (2). We follow the approach of ref. [12]. The relevant partonic processes, shown in fig. 2, are those in which the quark emits a hard gluon or those initiated by gluons:

$$\gamma^* + q \to q + g \quad \gamma^* + q \to g + q \quad \gamma^* + g \to q + \bar{q}\,. \qquad (8)$$

It is clear that now, contrary to the lowest-order QED process, $\gamma^* + q \to q$, the final parton can have a large transverse momentum, even starting from a collinear configuration. Such a contribution certainly dominates the production of hadrons with large P_T values.

One introduces the parton variables x' and z', defined similarly to the hadronic variables x_{Bj} and z_h,

$$x' = \frac{Q^2}{2k\cdot q} = \frac{x_{Bj}}{\xi}\,, \qquad z' = \frac{k\cdot k'}{k\cdot q} = \frac{z_h}{\zeta}\,, \qquad (9)$$

where k and k' are the four-momenta of the incident and fragmenting partons, respectively. ξ and ζ are the usual light-cone momentum fractions, which, in the collinear configuration with massless partons are given by $k = \xi P$ and $P_h = \zeta k'$. We denote by $\boldsymbol{p}_T$ (not to be confused with $\boldsymbol{p}_\perp$) the transverse momentum, with respect to the γ^*-direction, of the final fragmenting parton, $\boldsymbol{P}_T = \zeta\boldsymbol{p}_T$.

The semi-inclusive DIS cross-section, in the QCD parton model with collinear configuration, can be written, in general, as:

$$\frac{\mathrm{d}^5\sigma^{lp\to lhX}}{\mathrm{d}x_{Bj}\mathrm{d}y\,\mathrm{d}z_h\,\mathrm{d}^2\boldsymbol{P}_T} =$$
$$\sum_{i,j}\int \mathrm{d}x'\,\mathrm{d}z'\,\mathrm{d}^2\boldsymbol{p}_T\,\mathrm{d}\xi\,\mathrm{d}\zeta\delta\left(x_{Bj}-\xi x'\right)\delta\left(z_h-\zeta z'\right)$$
$$\times\delta^2(\mathbf{P}_T-\zeta\boldsymbol{p}_T)f_i\big(\xi,Q^2\big)\,\frac{\mathrm{d}\hat{\sigma}_{ij}}{\mathrm{d}x'\,\mathrm{d}y\,\mathrm{d}z'\,\mathrm{d}^2\boldsymbol{p}_T}D_j^h\left(\zeta,Q^2\right). \qquad (10)$$

To first order in α_s the partonic cross-section is given by [17,12]

$$\frac{\mathrm{d}\hat{\sigma}_{ij}}{\mathrm{d}x'\,\mathrm{d}y\,\mathrm{d}z'\,\mathrm{d}^2\boldsymbol{p}_T} = \frac{\alpha^2 e_q^2}{16\pi^2 Q^4}\,y\,L_{\mu\nu}M_{ij}^{\mu\nu}$$
$$\times\delta\left(p_T^2-\frac{z'}{x'}(1-x')(1-z')Q^2\right), \qquad (11)$$

where ij denote the initial and fragmenting partons, $ij = qq, qg, gq$. Inserting the above expression into eq. (10) yields, for the $\mathcal{O}(\alpha_s)$ cross-section:

$$\frac{\mathrm{d}^5\sigma_1^{lp\to lhX}}{\mathrm{d}x_{Bj}\mathrm{d}y\,\mathrm{d}z_h\,\mathrm{d}^2\boldsymbol{P}_T} = \frac{\alpha^2\,e_q^2}{16\pi^2}\,\frac{y}{Q^4}\int_{x_{Bj}}^1\frac{\mathrm{d}x'}{x'P_T^2+z_h^2(1-x')Q^2}$$
$$\times\sum_{i,j} f_i\Big(\frac{x_{Bj}}{x'},Q^2\Big)L_{\mu\nu}\,M_{ij}^{\mu\nu}\,D_j^h\left(z_h+\frac{x'P_T^2}{z_h(1-x')Q^2},Q^2\right), \qquad (12)$$

with [12]

$$L_{\mu\nu}M_{qq}^{\mu\nu} = \frac{64\pi}{3}Q^2\frac{(l\cdot k)^2+(l'\cdot k')^2+(l'\cdot k)^2+(l\cdot k')^2}{(k\cdot k'')(k'\cdot k'')}$$
$$= \frac{64\pi}{3}\,\frac{Q^2}{y^2}\left\{[1+(1-y)^2]\left[(1-x')(1-z')\right.\right.$$
$$\left.+\frac{1+(x'z')^2}{(1-x')(1-z')}\right]+8\,x'z'\,(1-y)$$
$$-4\sqrt{\frac{x'z'\,(1-y)}{(1-x')(1-z')}}\,(2-y)$$
$$\times[x'z'+(1-x')(1-z')]\cos\phi_h$$
$$\left.+\,4\,x'z'\,(1-y)\,\cos 2\phi_h\right\}, \qquad (13)$$

$$L_{\mu\nu}M_{qg}^{\mu\nu} = \frac{64\pi}{3}Q^2\frac{(l\cdot k)^2+(l'\cdot k'')^2+(l'\cdot k)^2+(l\cdot k'')^2}{(k\cdot k')(k'k'')}$$
$$= \frac{64\pi}{3}\frac{Q^2}{y^2}\Bigg\{[1+(1-y)^2]\Bigg[(1-x')z' + \frac{1+x'^2(1-z')^2}{(1-x')z'}\Bigg] + 8\,x'(1-y)(1-z') + 4\sqrt{\frac{x'(1-y)(1-z')}{(1-x')z'}}\,(2-y) \times[x'(1-z')+(1-x')z']\cos\phi_h + 4\,x'(1-y)(1-z')\cos 2\phi_h\Bigg\}, \quad (14)$$

$$L_{\mu\nu}M_{gq}^{\mu\nu} = \frac{64\pi}{3}Q^2\frac{(l\cdot k'')^2+(l'\cdot k')^2+(l'\cdot k'')^2+(l\cdot k')^2}{(k\cdot k')(k\cdot k'')}$$
$$= 8\pi\alpha_s\frac{Q^2}{y^2}\Bigg\{[1+(1-y)^2]\,[x'^2+(1-x')^2] \frac{z'^2+(1-z')^2}{z'(1-z')} + 16\,x'(1-x')(1-y) - 4\sqrt{\frac{x'(1-x')(1-y)}{z'(1-z')}}\,(2-y) \times(1-2x')(1-2z')\cos\phi_h + 8\,x'(1-x')(1-y)\cos 2\phi_h\Bigg\}, \quad (15)$$

where we have explicitely written the scalar products in terms of x', y, z' and $\cos\phi_h$. Notice the appearance of the $\cos\phi_h$ and $\cos 2\phi_h$ terms: ϕ_h is the azimuthal angle of the fragmenting partons, which, in a collinear configuration, concides with the azimuthal angle of the detected final hadron. The above expressions agree with results previously obtained in the literature [17].

Large values of P_T cannot be generated by the modest amount of intrinsic motion [1]; we expect that eq. (12) will dominantly describe the cross-sections for the lepto-production of hadrons with P_T values above 1 (GeV/c).

Let us finally briefly consider the contributions of order α_s^2 (NLO), $\mathrm{d}\sigma_2$ in eq. (2). These, for the production of large-P_T hadrons, have been recently computed [13,14], resulting in large corrections to the $\mathcal{O}(\alpha_s)$ (LO) results, and leading to a good agreement with experimental data. It would be unnecessarily complicated, for our purposes, to take exactly into account these contributions, as we have done for the LO ones, via eqs. (12)–(15). The most simple way of inserting the NLO results in our study is via the K-factor, defined as the NLO to LO ratio of the SIDIS cross-sections. A close examination of the K-factor shows a clear dependence on P_T and the other kinematical variables: for example, it may be larger than 10 at low P_T and Q^2, while approaching unity at larger values (see, for example, fig. 3 of ref. [13]). However, we shall need to use the K-factor only in limited ranges of P_T (up to 3 GeV/c at most) and Q^2, depending on the sets of experimental data we consider: in these limited kinematical regions we find that a satisfactory description of the SIDIS experimental data can be achieved by using constant values of K, which will be indicated in each case.

Therefore, we will effectively include $\mathcal{O}(\alpha_s^2)$ contributions in our computations by writing eq. (2) as

$$\mathrm{d}\sigma = \alpha_s^0\mathrm{d}\sigma_0 + \alpha_s^1\,K\,\mathrm{d}\sigma_1 + \ldots, \quad (16)$$

where $\mathrm{d}\sigma_0$ and $\mathrm{d}\sigma_1$ are calculated according to eqs. (4) and (12), respectively. The first term dominates at $P_T \lesssim 1$ GeV/c, and the second one at $P_T \gtrsim 1$ GeV/c.

3 Numerical results

In ref. [1] several sets of experimental data, showing the explicit dependence of the SIDIS unpolarized cross-sections on the azimuthal angle ϕ_h and on P_T, were considered. A comprehensive fit, based on, eq. (4) —or its simplified version valid up to $\mathcal{O}(k_\perp/Q)$, eq. (7)— was performed, in order to determine the values of $\langle k_\perp^2\rangle$ and $\langle p_\perp^2\rangle$, obtaining

$$\langle k_\perp^2\rangle = 0.25\ (\mathrm{GeV})^2\,, \qquad \langle p_\perp^2\rangle = 0.20\ (\mathrm{GeV})^2\,. \quad (17)$$

These values were assumed to be constant and flavour independent. We have explicitely checked that introducing x, z-dependences in $\langle k_\perp^2\rangle$ and $\langle p_\perp^2\rangle$, while complicating the numerics, does not significantly change our results, since the x and z ranges of the experiments we consider are limited. This was discussed in ref. [1].

The study of ref. [1] also showed clearly that eq. (4) —zeroth-order pQCD with TMD distribution and fragmentation function— works very well in the $P_T \simeq \Lambda_{\mathrm{QCD}} \simeq k_\perp$ region, but fails at larger P_T values, where higher-order pQCD contributions, with collinear partonic configurations, are expected to take over and explain the data. The transition point is around $P_T \simeq 1$ GeV/c.

We have redone the analysis of ref. [1] taking into account, in the appropriate kinematical regions, also the pQCD contributions. It turns out that, while a complete description of the data in the full P_T range is possible, a little variation is required to the values given in eq. (17). Actually, the resulting change is included within a 20% variation of the parameters, already considered in ref. [1].

Figures 3–7 show our results obtained by adding, according to eq. (16), the contributions of eq. (4) to the contributions (computed above $P_T = 1$ GeV/c) of eq. (12). We have used

$$\langle k_\perp^2\rangle = 0.28\ (\mathrm{GeV})^2\,, \qquad \langle p_\perp^2\rangle = 0.25\ (\mathrm{GeV})^2\,, \quad (18)$$

again constant and flavour independent. The K-factor was fixed to be a constant, with different values according to the different P_T and Q^2 ranges involved. Here, and throughout the paper we have adopted the MRST01

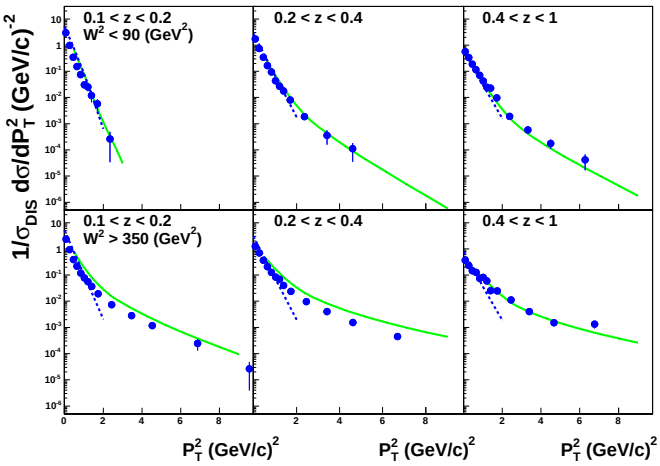

Fig. 3. The normalized cross-section $\mathrm{d}\sigma/\mathrm{d}P_T^2$: the dashed line reproduces the $\mathcal{O}(\alpha_s^0)$ contributions, computed by taking into account the partonic transverse intrinsic motion at all orders in $(k_\perp/Q)$, eq. (4). The solid line corresponds to collinear and pQCD contributions, computed at LO, with a K-factor ($K = 6$) to account for NLO effects, eqs. (12)–(16). The data are from EMC Collaboration measurements [20]. $\langle k_\perp \rangle$ and $\langle p_\perp \rangle$ are fixed as in eq. (18).

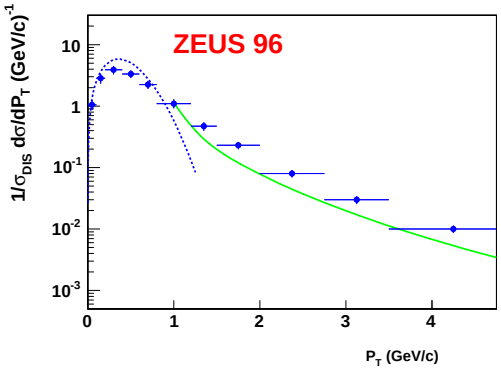

Fig. 4. The normalized cross-section $\mathrm{d}\sigma/\mathrm{d}P_T$: the dashed line reproduces the $\mathcal{O}(\alpha_s^0)$ contribution, computed by taking into account the partonic transverse intrinsic motion at all orders in the $(k_\perp/Q)$ expansion, eq. (4); the solid line corresponds to the SIDIS cross-section as given by LO contributions and a K-factor ($K = 1.5$) to account for NLO effects, eqs. (12)–(16). The data are from ZEUS Collaboration measurements [21]. $\langle k_\perp \rangle$ and $\langle p_\perp \rangle$ are fixed as in eq. (18).

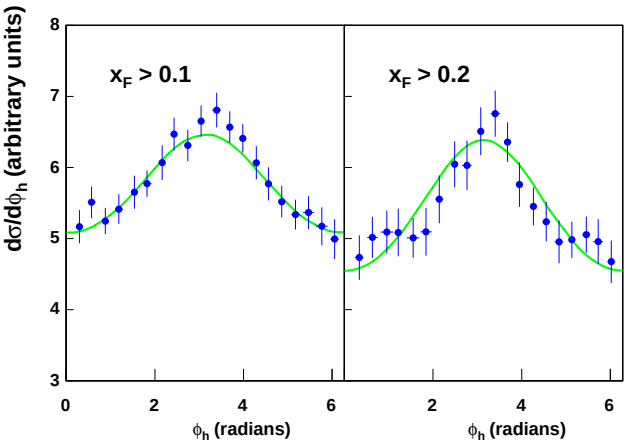

Fig. 5. The cross-section $\mathrm{d}\sigma/\mathrm{d}\phi_h$: the solid line is obtained by including all orders in $(k_\perp/Q)$, the LO corrections and a $K = 6$ factor to account for NLO effects. The data are from EMC measurements [9]. $\langle k_\perp \rangle$ and $\langle p_\perp \rangle$ are fixed as in eq. (18).

NLO [18] set of distribution functions and the fragmentation functions by Kretzer [19] at NLO.

Let us comment in greater detail on each single plot. In fig. 3 we compare our results to the EMC measurements of the SIDIS P_T^2 distributions (normalized to the integrated DIS cross-section) [20], defined as

$$\frac{1}{\sigma_{\rm DIS}}\frac{\mathrm{d}\sigma}{\mathrm{d}P_T^2} = \frac{1}{2\sigma_{\rm DIS}} \int \mathrm{d}\phi_h \, \mathrm{d}x_{Bj} \, \mathrm{d}y \, \mathrm{d}z_h \frac{\mathrm{d}^5\sigma^{\ell p\to \ell h X}}{\mathrm{d}x_{Bj} \, \mathrm{d}y \, \mathrm{d}z_h \, \mathrm{d}^2\boldsymbol{P}_T}\,, \tag{19}$$

where the integration covers the x_{Bj}, y, z_h and P_T regions consistent with the experimental cuts:

$$Q^2 > 5\ (\mathrm{GeV}/c)^2\,, \qquad E_h > 5\ (\mathrm{GeV}),$$
$$0.1 < z_h < 1, \qquad 0.2 < y < 0.8\,.$$

The dashed lines reproduce the $\mathcal{O}(\alpha_s^0)$ contribution, computed by taking into account the partonic transverse intrinsic motion at all orders in $(k_\perp/Q)$, whereas the solid lines correspond to the SIDIS cross-section as obtained by including LO corrections and the K-factor ($K = 6$) to account for NLO effects. The two contributions together give a very good complementary description of the data over the full P_T domain. Unavoidably, there is a slight mismatch at the transition point, $P_T = 1\,\mathrm{GeV}/c$, where both contributions somewhat describe the same physics, and some kind of average should be performed to avoid double counting. The value $K = 6$ is the simplest, although rough, approximation, in the kinematical range of the data considered here, to the computed K-factor (see, fig. 3 of ref. [13]). $\sigma_{\rm DIS}$ is evaluated starting from eq. (17) of ref. [1]; pQCD corrections for this integrated quantity are negligible.

A similar very good agreement, shown in fig. 4, is obtained when comparing our computations with the experimental measurements of the ZEUS Collaboration at DESY [21]. Here, the SIDIS differential cross-section,

$$\frac{1}{\sigma_{\rm DIS}}\frac{\mathrm{d}\sigma}{\mathrm{d}P_T} = \frac{1}{\sigma_{\rm DIS}} \int \mathrm{d}\phi_h \mathrm{d}x_{Bj} \mathrm{d}Q^2 \mathrm{d}z_h P_T \frac{\mathrm{d}^5\sigma^{\ell p\to \ell h X}}{\mathrm{d}x_{Bj} \mathrm{d}Q^2 \mathrm{d}z_h \mathrm{d}^2\boldsymbol{P}_T}\,, \tag{20}$$

is obtained by performing the integrations according to the following experimental conditions:

$$10 < Q^2 < 160\ (\mathrm{GeV}/c)^2\,, \quad 75 < W < 175\ (\mathrm{GeV}), \tag{21}$$

and the K-factor is taken to be 1.5 (as shown in fig. 8 of ref. [13]).

In fig. 5 we compare our results to the EMC measurements of the (not normalized) ϕ_h distributions [9],

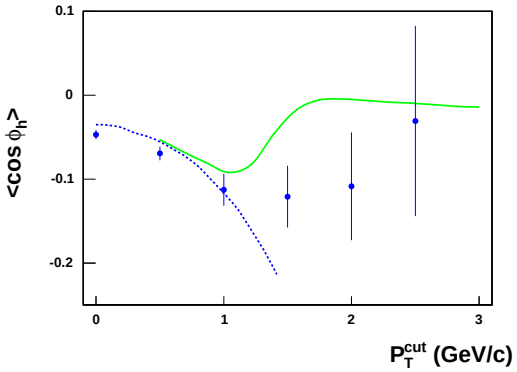

Fig. 6. $\langle \cos\phi_h \rangle$ as a function of P_T^{cut}: the dashed line reproduces the $\mathcal{O}(\alpha_s^0)$ contribution, computed by taking into account the partonic transverse intrinsic motion at all orders in $(k_\perp/Q)$; the solid line corresponds to the SIDIS cross-section as obtained by including LO corrections and a $K = 6$ factor to account for NLO effects. The data are from the E665 Collaboration [10].

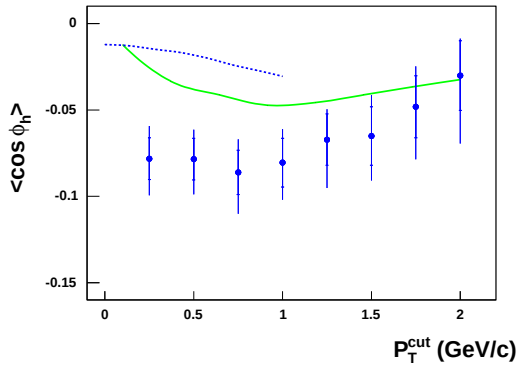

Fig. 7. $\langle \cos\phi_h \rangle$ as a function of P_T^{cut}: the dashed line reproduces the $\mathcal{O}(\alpha_s^0)$ contribution, computed by taking into account the partonic transverse intrinsic motion at all orders in $(k_\perp/Q)$; the solid line corresponds to the SIDIS cross-section as obtained by including LO corrections and a $K = 1.5$ factor to account for NLO effects. The data are from the ZEUS Collaboration [22].

proportional to

$$\frac{\mathrm{d}\sigma^{\ell p\to \ell h X}}{\mathrm{d}\phi_h} = \int \mathrm{d}x_{Bj}\,\mathrm{d}y\,\mathrm{d}z_h\,P_T\,\mathrm{d}P_T\,\frac{\mathrm{d}^5\sigma^{\ell p\to \ell h X}}{\mathrm{d}x_{Bj}\mathrm{d}y\,\mathrm{d}z_h\,\mathrm{d}^2\boldsymbol{P}_T}\,. \tag{22}$$

The integration regions are fixed by the conditions

$$x_F > 0.1, \qquad P_T > 0.2\ (\mathrm{GeV}/c),$$
$$0.2 < y < 0.8, \qquad Q^2 > 4\ (\mathrm{GeV}/c)^2\,,$$

where $x_F = 2P_L/W$ and P_L is the longitudinal momentum of the produced hadron relative to the virtual photon.

This is a quantity integrated over $P_T \geq 0.2\,\mathrm{GeV}/c$; we have used only $\mathrm{d}\sigma_0$ up to $P_T = 1\,\mathrm{GeV}/c$ and added the $K\,\mathrm{d}\sigma_1$ contributions (with $K = 6$) above that. We notice, however, that the dominant contributions come from very low P_T's, while the pQCD contribution is almost negligible.

Figures 6 and 7 show our predictions for the average value of $\cos\phi_h$ compared to the experimental data from the FNAL E665 Collaboration [10] (μp and μd interactions at 490 GeV) and from the ZEUS Collaboration [22] (positron-proton collisions at 300 GeV) respectively. Here $\langle \cos\phi_h \rangle$ is defined as

$$\langle \cos\phi_h \rangle = \frac{\int \mathrm{d}x_{Bj}\mathrm{d}Q^2\mathrm{d}z_h\mathrm{d}^2\boldsymbol{P}_T\,\cos\phi_h\,\mathrm{d}^5\sigma}{\int \mathrm{d}x_{Bj}\mathrm{d}Q^2\mathrm{d}z_h\mathrm{d}^2\boldsymbol{P}_T\,\mathrm{d}^5\sigma}\,, \tag{23}$$

where $\mathrm{d}^5\sigma$ denotes the fully differential cross-section

$$\mathrm{d}^5\sigma \equiv \frac{\mathrm{d}^5\sigma^{\ell p\to \ell h X}}{\mathrm{d}x_{Bj}\,\mathrm{d}Q^2\,\mathrm{d}z_h\,\mathrm{d}^2\boldsymbol{P}_T}\,. \tag{24}$$

For the FNAL E665 data sample the integral over P_T runs from P_T^{cut} to $P_T^{max} \sim 10\,\mathrm{GeV}/c$ and the range of the other variables is fixed by the following experimental cuts:

$$Q^2 > 3\ (\mathrm{GeV})^2\,, \qquad 300 < W^2 < 900\ (\mathrm{GeV})^2\,,$$
$$60 < \nu < 500\ (\mathrm{GeV})\,, \qquad E_h > 8\ (\mathrm{GeV}),$$
$$0.1 < y < 0.85, \tag{25}$$

whereas for the ZEUS data sample the integral over P_T runs from P_T^{cut} to $P_T^{max} \sim 10\,\mathrm{GeV}/c$, within the ranges

$$0.01 < x_{Bj} < 0.1, \qquad 0.2 < y < 0.8,$$
$$0.2 < z_h < 1.0, \qquad 180 < Q^2 < 7220\ (\mathrm{GeV})^2\,. \tag{26}$$

As in the previous case, we have added perturbative corrections only from $P_T = 1\ (\mathrm{GeV}/c)$, leaving $\mathrm{d}\sigma_0$ to be the only contributing term for values of P_T below 1 (GeV/c).

The results we obtain are in good qualitative agreement with the FNAL E665 experimental data. As expected, they show that the pQCD contributions are very small at low P_T^{cut} values, but quickly increase as P_T^{cut} raises, significantly correcting the fast fall of the $\mathcal{O}(\alpha_s^0)$ term, as shown in fig. 6.

Instead, our results disagree with the ZEUS data, especially in the lower range of P_T^{cut}. This is surprising and would deserve further experimental studies. The $\cos\phi_h$ modulation, at small P_T values, is a kinematical higher-twist effect, and decreases like P_T/Q for growing values of Q, as shown in eq. (7). Therefore we expect, and indeed we find, $\langle \cos\phi_h \rangle$ to be much smaller for ZEUS data, which correspond to huge values of Q^2, than for E665 results, which correspond to much lower Q^2 values.

We have also computed, with the same procedure, $\langle \cos(2\phi_h) \rangle$. We have seen that such a dependence can arise both, at $\mathcal{O}(P_T/Q)^2$, from intrinsic motion, and, at $\mathcal{O}(\alpha_s)$, from pQCD corrections. However, there is another non-perturbative, leading-twist, small-P_T source of the $\cos(2\phi_h)$-dependence, related to the combined action of the Boer-Mulders [23] and Collins [24] effects; this has been studied in ref. [25] and, recently, in ref. [26], where both the $1/Q^2$ kinematical contribution and the Boer-Mulders $\otimes$ Collins one were studied and found to be of comparable size. Therefore, our results, which ignore the Boer-Mulders $\otimes$ Collins contribution, can be considered reliable only in the large-P_T region; indeed, in this region, we find agreement with the ZEUS experimental data of ref. [22], as shown in fig. 8.

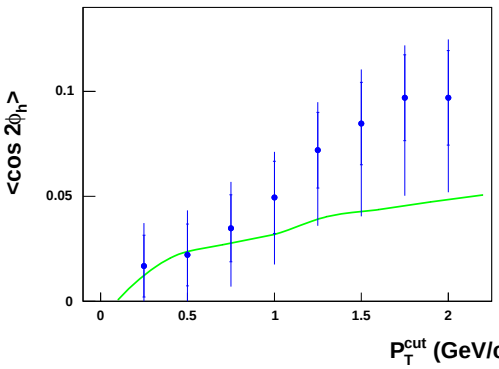

Fig. 8. $\langle\cos(2\phi_h)\rangle$ as a function of P_T^{cut} as obtained by including LO corrections and a $K = 1.5$ factor to account for NLO effects. The data are from the ZEUS Collaboration [22].

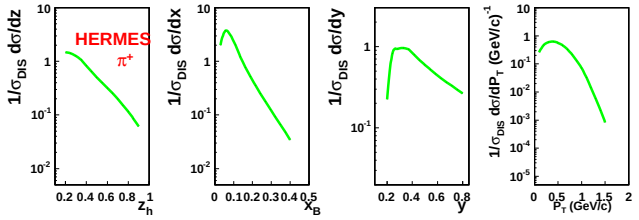

Fig. 9. Predictions for the normalized SIDIS cross-section corresponding to the production of π^+ as it will be measured by the HERMES Collaboration in the forthcoming future. The solid lines correspond to the SIDIS cross-section as obtained by including all orders in the $(k_\perp/Q)$ expansion. Notice that QCD corrections have no influence in this range of low P_T's.

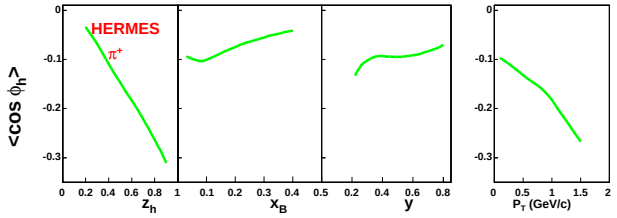

Fig. 10. Predictions for $\langle\cos\phi_h\rangle$ corresponding to the production of π^+ as it will be measured by the HERMES Collaboration in the forthcoming future. The solid lines correspond to $\langle\cos\phi_h\rangle$ we find by including all orders in the $(k_\perp/Q)$ expansion. Notice that QCD corrections have no influence in this range of low P_T's.

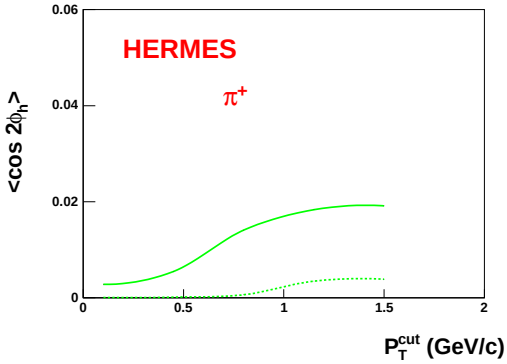

Fig. 11. Predictions for $\langle\cos 2\phi_h\rangle$ corresponding to the production of π^+ as it will be measured by the HERMES Collaboration in the forthcoming future. The solid line is obtained by including all contributions and all orders in the $(k_\perp/Q)$ expansion. The dashed line corresponds to the perturbative QCD contributions only.

4 Predictions for forthcoming measurements

New data are expected from ongoing measurements or data analysis at HERMES, COMPASS and JLab. They concern dominantly the small-P_T (and, hopefully, large enough Q^2) region, where we have seen that the simple partonic approach, with unintegrated distribution and fragmentation functions, can give a very satisfactory description of the available data. We can easily give detailed predictions which can soon be tested, allowing a further check on the role of intrinsic motions in affecting physical observables. We consider the SIDIS cross-sections and the average value of $\cos\phi_h$. Also $\langle\cos 2\phi_h\rangle$, keeping in mind the comments at the end of the previous section, is computed.

In fig. 9, we plot the SIDIS cross-section, for π^+ production at HERMES, as a function of one variable at a time, either z_h, x_{Bj}, y or P_T; the integration over the unobserved variables has been performed consistently with the setup of the HERMES experiment, which studies the scattering of positrons at $p_{lab} = 27.57\,\mathrm{GeV}/c$ against a fixed hydrogen gas target:

$$Q^2 > 1\ (\mathrm{GeV}/c)^2, \quad W^2 > 10\,\mathrm{GeV}^2, \quad P_T > 0.05\,\mathrm{GeV}/c,$$
$$0.023 < x_{Bj} < 0.4, \quad 0.2 < z_h < 0.7, \quad 0.1 < y < 0.85,$$
$$2 < E_h < 15\,\mathrm{GeV}. \qquad (27)$$

In these kinematical regions the cross-section is heavily dominated by the $\mathrm{d}\sigma_0$ term of eq. (2), computed according to eq. (4); σ_{DIS} is computed according to eq. (17) of ref. [1]. We also evaluate the average value of $\cos\phi_h$ in the same kinematical region, shown in fig. 10, and of $\cos 2\phi_h$, shown in fig. 11. The latter, however, can only be taken as a partial (higher-twist) contribution to the real $\langle\cos 2\phi_h\rangle$, as explained at the end of the last section.

We notice that very similar predictions, for the cross-section, $\langle\cos\phi_h\rangle$ and $\langle\cos 2\phi_h\rangle$, are obtained for π^0 and π^- production, which we do not show.

The COMPASS experiment at CERN collects data in $\mu d \to \mu h^\pm X$ processes at $p_{lab} = 160\,\mathrm{GeV}/c$, covering the following kinematical regions:

$$Q^2 > 1\ (\mathrm{GeV}/c)^2, \quad W^2 > 25\,\mathrm{GeV}^2, \quad P_T > 0.1\,\mathrm{GeV}/c,$$
$$E_h < 15\,\mathrm{GeV}, \quad 0.2 < z_h < 1, \quad 0.1 < y < 0.9. \qquad (28)$$

Figure 12 shows our corresponding predictions for the SIDIS cross-section —for the production of positively charged hadrons— as a function of the kinematical variables z_h, x_{Bj}, y and P_T, as obtained from eq. (4). Notice that we neglect nuclear corrections and use the isospin symmetry in order to obtain the parton distribution functions of the deuterium. Predictions for $\langle\cos\phi_h\rangle$ are

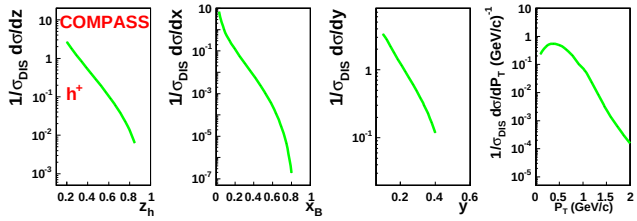

Fig. 12. Predictions for the normalized SIDIS cross-section corresponding to the production of positively charged hadrons as it will be measured by the COMPASS Collaboration in the forthcoming future. The solid lines correspond to the SIDIS cross-section as obtained by including all orders in the $(k_\perp/Q)$ expansion.

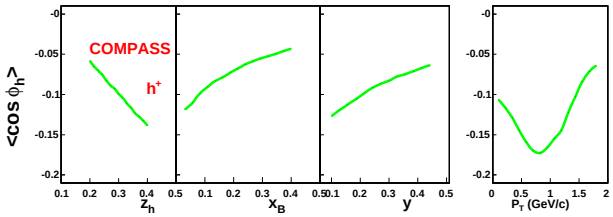

Fig. 13. Predictions for $\langle\cos\phi_h\rangle$ corresponding to the production of positively charged hadrons as it will be measured by the COMPASS Collaboration in the forthcoming future. The solid lines correspond to $\langle\cos\phi_h\rangle$ we find by including all orders in the $(k_\perp/Q)$ expansion.

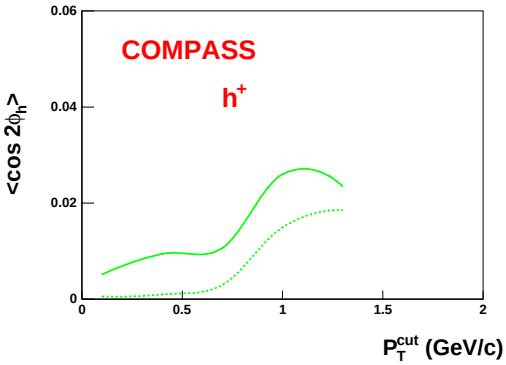

Fig. 14. Predictions for $\langle\cos 2\phi_h\rangle$ corresponding to the production of positively charged hadrons as it will be measured by the COMPASS Collaboration in the forthcoming future. The solid line is obtained by including all contributions and all orders in the $(k_\perp/Q)$ expansion. The dashed line corresponds to the perturbative QCD contributions only.

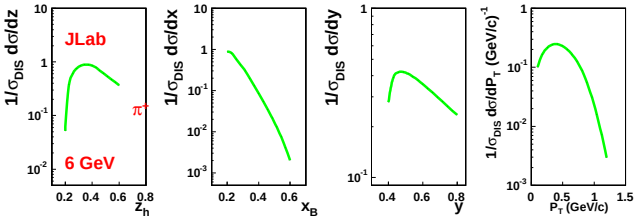

Fig. 15. Predictions for the normalized SIDIS cross-section corresponding to the production of π^+ as it will be measured by the JLab Collaboration in the forthcoming future. The solid lines correspond to the SIDIS cross-section as obtained by including all orders in the $(k_\perp/Q)$ expansion. Notice that QCD corrections have no influence in this range of low P_T's.

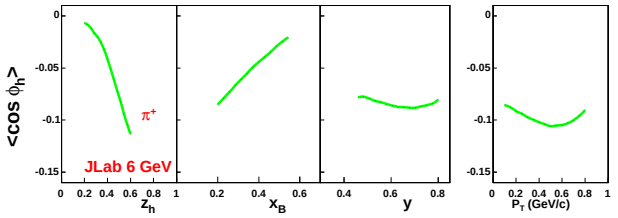

Fig. 16. Predictions for $\langle\cos\phi_h\rangle$ corresponding to the production of π^+ as it will be measured by the JLab Collaboration in the forthcoming future. The solid lines correspond to $\langle\cos\phi_h\rangle$ we find by including all orders in the $(k_\perp/Q)$ expansion. Notice that QCD corrections have no influence in this range of low P_T's.

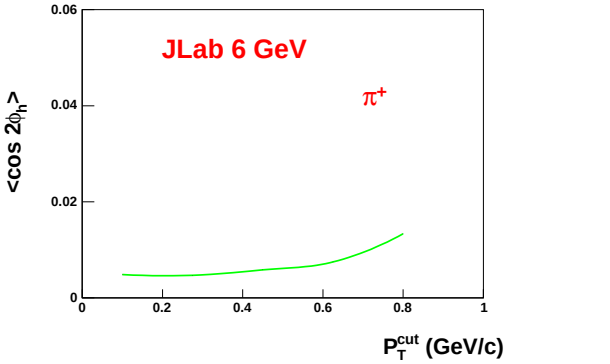

Fig. 17. Predictions for $\langle\cos 2\phi_h\rangle$ corresponding to the production of π^+ as it will be measured by the JLab Collaboration in the forthcoming future. The solid lines correspond to $\langle\cos 2\phi_h\rangle$ we find by including all orders in the $(k_\perp/Q)$ expansion. Notice that QCD corrections have no influence in this range of low P_T's.

presented in fig. 13 and the higher-twist contributions to $\langle\cos 2\phi_h\rangle$ in fig. 14, where QCD corrections (dashed line) are also shown for comparison. Notice that, in contrast to the HERMES case, the perturbative QCD corrections are relatively important, as COMPASS data can reach higher P_T values. The transition from the non-perturbative to the perturbative regime, which takes place at $P_T \sim 1\,\text{GeV}$, is in fact well visible in the right panel of fig. 13.

Finally, JLab collects and will collect data in the collisions of 6 and 12 GeV electrons from a fixed He^3 target. In this case the relevant kinematical regions are the following:

$$Q^2 > 1\ (\text{GeV}/c)^2\,, \quad W^2 > 4\,\text{GeV}^2\,, \quad P_T > 0.1\,\text{GeV}/c,$$
$$1.0 < E_h < 3.5\,\text{GeV}, \quad 0.4 < z_h < 0.7, \quad 0.1 < x_{Bj} < 0.6$$
$$0.4 < y < 0.85. \tag{29}$$

Our results for the corresponding SIDIS cross-sections, $\langle\cos\phi_h\rangle$ and $\langle\cos 2\phi_h\rangle$ are shown in figs. 15, 16 and 17 respectively: as for the previous experiments, also the JLab data are dominated by $\mathcal{O}(\alpha_s^0)$ terms and are almost completely insensitive to the LO and NLO perturbative QCD

corrections. Again, we show results for π^+ production, but very similar ones hold for π^- and π^0, which we do not show.

All these results depend on intrinsic momenta, both $\boldsymbol{k}_\perp$ in the partonic distributions and $\boldsymbol{p}_\perp$ in the quark fragmentation. This is obvious for quantities like $\mathrm{d}\sigma/\mathrm{d}P_T$ and $\langle\cos\phi_h\rangle$ which could not even be defined, at $\mathcal{O}(\alpha_s^0)$, without intrinsic motion (and pQCD corrections are negligible for the experiments we consider). However, this is also true for the differential cross-sections in z, x_{Bj} and y: although they get contributions from intrinsic motion only at $\mathcal{O}(P_T/Q)^2$, as one can explicitly see from eq. (7), these contributions can be sizeable in the kinematical domains of HERMES, COMPASS and JLab.

5 Conclusions

We have considered the azimuthal and P_T-dependence of SIDIS data from low to large P_T; they both cannot be explained in the simple parton model ($\mathcal{O}(\alpha_s^0)$) with collinear configurations. They can originate from intrinsic motions and/or pQCD corrections. The outcome of our analysis turns out to be very simple: up to $P_T \lesssim 1\,\mathrm{GeV}/c$ the simple parton model with unintegrated distribution and fragmentation functions explains the data and leads to a good evaluation of $\langle k_\perp\rangle$ and $\langle p_\perp\rangle$, while at larger P_T values, $P_T \gtrsim 1\,\mathrm{GeV}/c$, the perturbative QCD contributions originating from hard gluonic radiation processes and elementary scattering initiated by gluons, are dominant.

Having clearly established the complementarity of the two approaches, and in particular having gained full confidence in the domain of applicability of the unintegrated parton model, we have given predictions for the cross-sections and for the values of $\langle\cos\phi_h\rangle$, as they will soon be measured by HERMES, COMPASS and JLab Collaborations, mainly in the low-P_T region. These new data will be a very important tool to test our knowledge of the intrinsic partonic internal motion and on the TMD quark distribution and fragmentation functions.

We acknowledge the support of the European Community —Research Infrastructure Activity under the FP6 "Structuring the European Research Area" programme (HadronPhysics, contract number RII3-CT-2004-506078).

References

1. M. Anselmino, M. Boglione, U. D'Alesio, A. Kotzinian, F. Murgia, A. Prokudin, Phys. Rev. D **71**, 074006 (2005).
2. R.N. Cahn, Phys. Lett. B **78**, 269 (1978); Phys. Rev. D **40**, 3107 (1989).
3. HERMES Collaboration (A. Airapetian *et al.*), Phys. Rev. Lett. **94**, 012002 (2005); M. Diefenthaler (on behalf of the HERMES Collaboration), e-Print Archive: hep-ex/0507013.
4. COMPASS Collaboration (V.Yu. Alexakhin *et al.*), Phys. Rev. Lett. **94**, 202002 (2005).
5. M. Anselmino, M. Boglione, U. D'Alesio, A. Kotzinian, F. Murgia, A. Prokudin, Phys. Rev. D **72**, 094007 (2005).
6. D. Sivers, Phys. Rev. D **41**, 83 (1990); **43**, 261 (1991).
7. X. Ji, J.-P. Ma, F. Yuan, Phys. Rev. D **71**, 034005 (2005).
8. EMC Collaboration (J.J. Aubert *et al.*), Phys. Lett. B **130**, 118 (1983).
9. EMC Collaboration (M. Arneodo *et al.*), Z. Phys. C **34**, 277 (1987).
10. Fermilab E665 Collaboration (M.R. Adams *et al.*), Phys. Rev. D **48**, 5057 (1993).
11. H. Georgi, H.D. Politzer, Phys. Rev. Lett. **40**, 3 (1978).
12. J. Chay, S.D. Ellis, W.J. Stirling, Phys. Rev. D **45**, 46 (1992).
13. B.A. Kniehl, G. Kramer, M. Maniatis, Nucl. Phys. B **711**, 345 (2005).
14. A. Daleo, D. de Florian, R. Sassot, Phys. Rev. D **71**, 034013 (2005).
15. X. Ji, J.-W. Qiu, W. Vogelsang, F. Yuan, e-Print Archive: hep-ph/0602239; Phys. Rev. D **73**, 094017 (2006).
16. X. Ji, J.-W. Qiu, W. Vogelsang, F. Yuan, Phys. Lett. B **638**, 178 (2006).
17. A. Mendez, Nucl. Phys. B **145**, 199 (1978); A. Konig, P. Kroll, Z. Phys. C **16**, 89 (1982).
18. A.D. Martin, R.G. Roberts, W.J. Stirling, R.S. Thorne, Phys. Lett. B **531**, 216 (2002).
19. S. Kretzer, Phys. Rev. D **62**, 054001 (2000).
20. EMC Collaboration (J. Ashman *et al.*), Z. Phys. C **52**, 361 (1991).
21. ZEUS Collaboration (M. Derrick *et al.*), Z. Phys. C **70**, 1 (1996).
22. ZEUS Collaboration (J. Breitweg *et al.*), Phys. Lett. B **481**, 199 (2000).
23. D. Boer, P.J. Mulders, Phys. Rev. D **57**, 5780 (1998).
24. J.C. Collins, Nucl. Phys. B **396**, 161 (1993).
25. Leonard P. Gamberg, Gary R. Goldstein, Karo A. Oganessyan, Phys. Rev. D **67**, 071504 (2003); **68**, 051501 (2003).
26. V. Barone, Z. Lu, B.-Q. Ma, Phys. Lett. B **632**, 277 (2006).